Selected Results of the Collaborative Research Center "Droplet Dynamics under Extreme Ambient Conditions" SFB-TRR 75

K. Schulte*[1], B. Weigand[1], C. Tropea[2]
[1] University of Stuttgart, Institute of Aerospace Thermodynamics, 70569 Stuttgart, Germany
[2] Technische Universität Darmstadt, Institute of Fluid Mechanics and Aerodynamics, 64287 Darmstadt, Germany
*Corresponding author: kathrin.schulte@itlr.uni-stuttgart.de

Abstract
A fundamental understanding of droplet dynamics is the critical prerequisite to the prediction of natural processes and the optimization of technical systems involving drops and sprays. The Collaborative Research Center (CRC) SFB-TRR 75 was established in January 2010 to focus on the dynamics of basic drop processes, and in particular on processes involving extreme boundary conditions, for example, near thermodynamic critical conditions, at very low temperatures, under strong electric fields or in situations involving extremely large gradients in the boundary conditions. The goal is to gain a profound physical understanding of the essential processes, which is the basis for new analytical and numerical descriptions for an improved prediction of large systems in nature or in technical applications. This joint initiative involves researchers from the faculties of Mathematics, Chemistry, Electrical Engineering, Mechanical Engineering and Computer Sciences at the University of Stuttgart, the TU Darmstadt, the TU Berlin, and the DLR (German Aerospace Center) in Lampoldshausen within 17 projects.
The topics pursued at the CRC include droplet collisions at different ambient conditions, the behaviour of supercooled droplets in clouds, the contribution of supercooled large droplets (SLD) to aircraft icing, atomization and vaporization of droplets at high pressures and temperatures, as occurring in future combustion systems, and trans-critical injection conditions of fuel with flash boiling in rocket combustion chambers.
This article provides an overview of the projects being carried out at the SFB-TRR 75 and highlights scientific results from selected projects. The main purpose of the paper is to familiarize colleagues with this extensive and dedicated research effort in this area of drop dynamics and to motivate and initiate future collaboration with others in this field.

Keywords
drop dynamics, extreme boundary conditions, spray combustion

Introduction

Many processes in nature and technological applications are influenced by droplet dynamics, such as rain or fuel injection into combustion chambers, but also highly advanced devices such as rocket engines or spray based production processes in the pharmaceutical industry.
The behaviour of droplets has been of scientific interest for a long time: Plateau [1] and Lord Rayleigh [2] studied drops under the influence of surface tension in the 19th century. While there are many scientific results available for both basic processes and complex systems, they often are restricted to moderate ambient conditions, e.g. [3], [4] and [5], However, many of the processes mentioned above take place under extreme ambient conditions. Under such extreme conditions, the prediction and simulation of drop behaviour is often unreliable. This holds for the near-critical or supercritical conditions in modern combustion engines as well as for thunderstorm clouds with their high electric fields or supercooled droplets that impinge on airplane wings, to name just a few examples. Due to the large effort in theoretical and numerical modelling and the required experimental equipment, much less research has been conducted in this field. There is also a lack of information about fluid properties and validation data for processes under extreme boundary conditions. These restrictions imply that in-depth research in this area not only demands the extensive development or improvement of experimental technologies and numerical models, but that inevitably a very close interaction of numerical and experimental research and the consequent involvement of expertise from fields like fluid data thermodynamics, fluid mechanics, mathematics, computer sciences, electronics and visualization are vital.
Therefore, in the particular area of drops under extreme conditions different topics were identified for further basic research, with the aim to improve our understanding and predictive capabilities of both naturally occurring and engineering systems involving droplets. This led to the conception of the present CRC (SFB-TRR 75), which combines the knowledge and experience of scientists from the above-mentioned subject areas.
Following the insight that complex droplet dynamic processes are determined by the interaction of very fundamental processes, the first 4-year period of the SFB-TRR 75 (2010-2013) was dedicated to the behaviour of single droplets.

During the second funding period (2014–2017), the physical understanding and the methodology gained in the first phase has been applied to small clusters of droplets to better understand their interaction. Selected results of the previous work in the SFB-TRR 75 can be found for example in [6-9]. Now in the final period of the CRC, research focusses on multi-droplet examples like sprays without, however, neglecting the development of the methods and fundamentals. In the current phase the CRC comprises 17 subprojects in 3 Research Areas - Research Area A: Methods and Fundamentals, Research Area B: Free Droplets, Research Area C: Droplets with Wall-Interactions.
In Research Area A numerical and analytical methods (TP-A2, TP-A3) are developed as well as methods for visualization (TP-A1), which are prerequisites for conducting the work in the other research areas. In TP-A4 basic droplet dynamic processes are investigated by molecular thermodynamics. In TP-A5 simulations of the mechanical deformation and movement of droplets on insulator surfaces with strong electric fields are investigated. The focus of TP-A7 is on the modelling and simulation of droplet collisions at high Weber numbers, varied ambient pressure and collisions of different miscible and non-miscible fluids.
In Research Area B free droplets are investigated. In TP-B1 dynamics and phase change of supercooled droplets in clouds are studied numerically and experimentally. TP-B2 investigates experimentally the evaporation of droplets under extreme thermodynamic conditions. The modelling and simulation of droplet evaporation in a foreign gas environment under trans-critical conditions is studied in TP-B3. The projects TP-B4 and TP-B5 investigate flash evaporation, e.g. for the transient injection of propellants into a rocket combustion chamber. TP-B6 studies evaporation processes with molecular dynamics simulation methods on the basis of atomistic interaction force field models.
In Research Area C droplet/wall interactions are investigated. In TP-C1 and TP-C2 special focus is placed on the three-phase contact line during droplet-wall interaction. In TP-C3 droplet/wall interactions are investigated for supercooled droplets on cold surfaces and in TP-C4 droplet/wall interaction is investigated for hot surfaces under high ambient pressures. TP-C5 deals with droplets under the influence of strong electrical fields. Selected results of TP-A2, TP-B4, TP-C1 and TP-C2 are presented in the following.

Results and Discussion

Development of numerical methods for the simulation of compressible droplet dynamic processes under extreme conditions

(TP-A2: T. Hitz, S. Jöns, C.D. Munz, Institute of Aerodynamics and Gas Dynamics, University of Stuttgart)

At extreme ambient conditions near the critical point, the often used assumption of an incompressible flow field is no longer valid. This is of major technical interest since modern fuel injection systems (e.g. in Diesel engines) operate at such conditions. However, in open literature only limited data for the near-critical conditions are available and many phenomena have not yet been completely understood.
Simulation of compressible multiphase flows meets three major difficulties with respect to the numerical approximation: First, an accurate method to describe the temporal evolution of the phase boundary as well as its interface properties is needed. Second, an accurate thermodynamic model is necessary to describe the fluid properties. The third difficulty is to develop an efficient method to resolve the physics at the phase interface. We propose a sharp-interface method and tackle the first challenge by capturing the phase boundary with a level-set method. The scheme is designed such that arbitrary equations of state can be used in the bulk phases to provide accurate material laws. The coupling at the interface is based on a modified ghost fluid method, where the fluxes are provided by the solution of an interface Riemann problem with the appropriate physical modeling.
The computational domain is divided by a sharp interface into two domains which contain the bulk phases. In each of the phases, the Navier-Stokes equations for a compressible fluid are solved with a high-order discontinuous Galerkin spectral element method (DGSEM) [10]. The DGSEM method comprises ideas taken from both finite-volume and finite-element methods. The domain is discretized by non-overlapping hexahedral elements. Inside each cell, a nodal polynomial solution ansatz of degree N is chosen, while discontinuities between each of the elements are permitted. The coupling between the elements is provided weakly by numerical flux functions, e.g. approximate Riemann solvers [11]. The temporal evolution of the solution polynomial is achieved through a high order explicit Runge-Kutta time stepping [12]. The DGSEM provides high order spatial accuracy as long as the solution is smooth. If discontinuities such as shock waves or phase boundaries occur, the solution polynomials start to oscillate due to Gibb's phenomenon and the simulation becomes unstable. To capture the discontinuities, a finite-volume sub-cell shock capturing is imposed [13]. Based on an indicator value, e.g. the level-set function for the phase boundary, the position of the discontinuity is detected. The element that contains the discontinuity then switches locally to a second order accurate finite volume (FV) formulation. The interpolation nodes are therefore redistributed equidistantly to obtain a Cartesian sub-grid.
The position of the phase interface is captured by a level-set method [14]. The level-set function is the signed distance function, where the zero iso-contour marks the phase interface position. The level-set equation is a standard linear advection equation, which is discretized using DGSEM. The polynomial degree of the level-set is $N_{LS} = N + 1$. This allows an accurate representation of the phase interface which is used to calculate geometrical

interface properties such as interface normals or curvature. The increased polynomial degree of the level-set function helps to reduce the amplitude of spurious currents. To guarantee continuous polynomials over a large stencil, we use a PnPm reconstruction [15] across the phase interface. The geometrical interface properties are then projected to the polynomial degree of the solution, N. To conserve the signed distance property of the level-set function, a reinitialization procedure is introduced. Based on the work of Sussman *et al.* [14], a Hamilton-Jacobi equation is solved with the WENO approach of Jiang and Peng [16]. A continuous velocity field for the advection of the level-set function is created by the extrapolation of the local phase interface velocity. Following Adalsteinsson and Sethian [17], a Hamilton-Jacobi equation is defined and solved using the same WENO scheme as for the reinitialization.

In the compressible multi-phase formulation, thermodynamics and hydrodynamics are closely linked. Typically, an equation of state (EOS) that is valid in the investigated near-critical range is complicated and, consequently, costly to evaluate. To accurately capture the fluid properties of the bulk phases, a tabulation approach for real gas equations of state is used [18]. The EOS is approximated by piecewise polynomials which are defined on a quadtree or octree structure in state space. The polynomial coefficients are calculated with a projection procedure based on the approach of Dumbser *et al.* [19]. To handle discontinuities in the equations of state, cut-cells are introduced at the liquid/vapor lines. The tabulation enables the use of highly accurate multiparameter EOS as provided, e.g., by the library CoolProp [20].

To keep the interface sharp, we use the ideas of the ghost fluid method that allow for a discrete separation of both bulk phases. Within the sharp interface approximation, the phase interface is shifted numerically from the level-set zero to the nearest grid boundary. At this location, the multiphase Riemann problem is solved, providing the proper jump conditions at the interface. These interface Riemann solvers (see e.g. [21], [22], [23], [24]) also allow for a straightforward inclusion of interface physics like surface tension forces, coupling of dissimilar equations of state and phase transition.

In case without phase transition, the phase boundary reduces to an impermeable material boundary, which is treated in the solution of the multiphase Riemann problem similarly as the contact discontinuity. Surface tension is explicitly considered by means of an additional pressure jump according to the Young-Laplace equation. We use a multiphase extension of the HLLC Riemann solver, developed by Hu *et al.* [25]. If phase transition occurs, the solution structure of the multiphase Riemann problem changes and a new wave is generated which represents the phase boundary. Across this wave, the two-phase jump conditions apply, and an additional condition has to be fulfilled to satisfy the second law of thermodynamics. This so-called kinetic relation takes information about the entropy production from the micro-scale. Furthermore, in case of phase transition, heat transfer across the phase boundary cannot be neglected such that the latent heat of evaporation is taken into account. Exact and approximate Riemann solvers were developed within the SFB-TRR 75 which consider the latent heat but neglect the heat transfer [22], [23]. Currently, methods are investigated to include both heat transfer and an appropriate kinetic relation in the solution of the multiphase Riemann problem.

In the following, we present a test case of a 2D liquid column in crossflow without phase transition. The simulation was conducted on a 2D Cartesian grid with 300×120 cells. The computational domain spans from $-2.5D_{ref}$ to $12.5D_{ref}$ in x-direction and $-3.0D_{ref}$ to $3.0D_{ref}$ in y-direction, where D_{ref} is the initial droplet diameter. Dirichlet boundary conditions were applied at the inlet. For the outlet a pressure outflow condition was chosen. The remaining boundaries of the domain are periodic. The polynomial degree of the solution was $N = 3$, the polynomial degree of the level-set solution was $N_{LS} = 4$.

The dimensionless quantities for this test case were chosen to be $Ma = |u_{air}|/c_{air} = 0.1$, $Re = \rho_{air}|u_{air}|\,D_{ref}/\mu_{air} = 200$ and $We = \rho_{air}u_{air}^2\,D_{ref}/\sigma = 1.67$. The speed of sound is given by $c_{air} = \sqrt{c_p/c_v p_{air}/\rho_{air}}$, where density and pressure are taken from initial state of the air and the material properties are given below. This way, the flow field remained subsonic and compressible effects, e.g. shock waves, were not present. The Reynolds number is large enough that Karman vortex shedding took place while the Weber number guaranties that the surface tension prevents a break-up of the droplet. The ideal gas and stiffened gas laws were used to describe the material behavior of the liquid and gas phases, respectively. Thus, the initial conditions could be chosen according to the dimensionless quantities. The initial solution in non-dimensional units read:

$$\boldsymbol{u} = \begin{cases} \boldsymbol{u_{air}} & for\ \sqrt{x^2+y^2} - D_{ref} < 0 \\ \boldsymbol{u_{liquid}} & for\ \sqrt{x^2+y^2} - D_{ref} > 0 \end{cases}, \tag{1}$$

with $\boldsymbol{u_{air}} = (\rho, \boldsymbol{v}, p)^T = \left(1.0\mathrm{kgm}^{-3}, 10\mathrm{ms}^{-1}, 0\mathrm{ms}^{-1}, 7142.856\mathrm{Pa}\right)^T$, and $\boldsymbol{u_{liquid}} = (1000\mathrm{kgm}^{-3}, 0\mathrm{ms}^{-1}, 0\mathrm{ms}^{-1}, 7262.856\mathrm{Pa})^T$. The liquid phase was modeled by the stiffened gas EOS, resembling liquid water at ambient conditions. The parameters were $c_{p,liquid} = 4267\ \mathrm{J(kgK)}^{-1}$, $c_{v,liquid} = 1816\ \mathrm{J(kgK)}^{-1}$, $\tilde{q} = 0\ \mathrm{J(kgK)}^{-1}$, $q = 0\ \mathrm{J \cdot kg}^{-1}$ and $p_\infty = 60993225.14\ \mathrm{Pa}$. The transport properties were $\lambda_{liquid} =$

$1.542\ \mathrm{W(mK)^{-1}}$ and $\mu_{liquid} = 2.5E-3\ \mathrm{kg(ms)^{-1}}$. The air was a perfect gas with $c_{p,air} = 1004.5\ \mathrm{J(kgK)^{-1}}$ and $c_{v,air} = 717.5\ \mathrm{J(kgK)^{-1}}$, the transport properties were $\lambda_{air} = 0.0707\ \mathrm{W(mK)^{-1}}$ and $\mu_{air} = 5E-5\ \mathrm{kg(ms)^{-1}}$. The surface tension was calculated from the given Weber number, leading to a value of $\sigma = 0.06\ \mathrm{Nm^{-1}}$. In this contribution, the focus lies on an interface model which is able to resolve surface tension. Thus, the multiphase HLLC solver was chosen to provide the fluxes for the ghost fluid method and phase transition effects were neglected. Time integration was performed by a fourth order low storage Runge-Kutta method under the stability criterion $CFL = 0.9$. The level-set was reinitialized every five time steps; the advection velocity field was extrapolated each time step. The simulation was performed on the Cray XC40 (Hazel Hen) at the High Performance Computing Center Stuttgart (HLRS) on 8 nodes and 192 processors in total. Figure 1 shows the vorticity of the solution at the non-dimensional time instance $t = 0.0025$. The liquid column was compressed by the gas flow and took an elongated shape. The Kármán vortices are clearly visible. The shedding started around the non-dimensional time instance $t = 0.0012$.

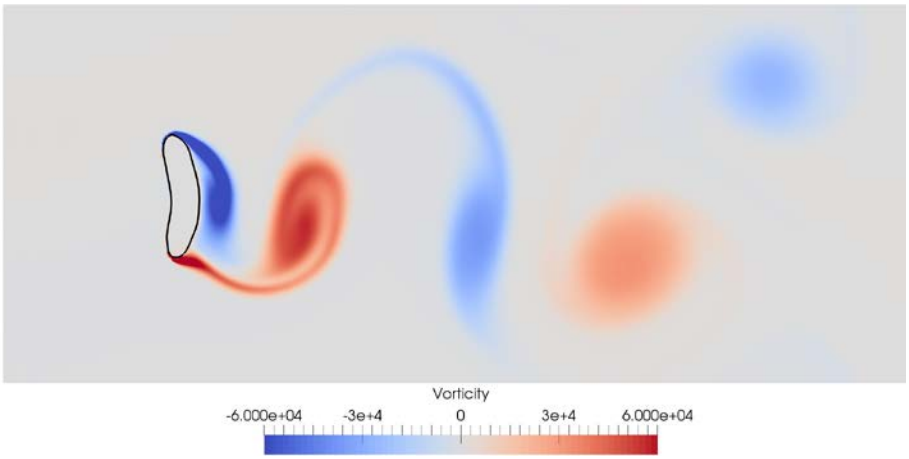

Figure 1. Two-dimensional simulation of a droplet in crossflow. The Reynolds number was Re=200 the Weber number was We=1.67, for which Kármán vortices and no droplet break up occurred as expected. The grid contained 300x120 elements and a polynomial degree of N=3 was used. The plot shows the velocity magnitude, the level-set zero is marked as the black line.

Experimental Investigation of Transient Injection Phenomena in Rocket Combustion Chambers under High Altitude Conditions with special Focus on Flash-Evaporation

(TP-B4: A. Rees, J. Sender, M. Oschwald, DLR, Institute of Rocket Propulsion, Lampoldshausen)

In the frame of future changes in propellant combinations and ignition methods, like e.g. laser ignition, for RCS (Reaction and Control System), OMS (Orbital and Manoeuvring System) and cryogenic upper stage engines, fluid flow structures and injection phenomena affecting ignition have to be investigated. One of these phenomena is the so-called flash evaporation, which is a sudden evaporation of a superheated liquid. TP-B4 focuses on the experimental investigation of superheated cryogenic liquids like LN2 (liquid nitrogen) and LOX (liquid oxygen) injected into a near vacuum atmosphere. Due to their superheated state the so-called flash-evaporation or flashing occurs, which is a sudden and violent jet breakup close to the injector outlet. The resulting spray is characterized by large spray angles and small droplet diameters.

After preliminary investigations of flashing LOX sprays presented at ILASS 2016 [7] a new cryogenic test bench M3.3 was constructed and put into operation during the second funding period of SFB-TRR 75. This test bench allows variable injection temperatures T_{inj} in the range of 77-120 K. It consists of three main systems: a media supply and pressurization system, the cryogenic temperature adjustment and injection system and the vacuum system, as depicted in Figure 2 on the left. In the supply and pressurization system all of the fluids necessary for operation of the test bench are focused from the general media infrastructure. The gas disposal of the test bench via release valves and pipes takes place here as well. Furthermore, in this system the used fluids nitrogen, oxygen and helium are reduced to the desired operation pressures before they are led to the cryogenic temperature adjustment and injection system. This system, which is the most important and complex one of the three main systems mentioned above, enables investigation of the influence of the injection temperature T_{inj} on the flash evaporation of LN2/LOX jets. This parameter together with the back pressure p_c, provided by the vacuum system, define the degree of superheat

$$\Delta T^* = \frac{T_{inj} - T_{sat}(p_c)}{T_{sat}(p_{inj}) - T_{sat}(p_c)} \qquad (2)$$

in terms of the saturation temperatures $T_{sat}(p_c)$ and $T_{sat}(p_{inj})$ at the back pressure p_c and the injection pressure p_{inj} or as the pressure ratio

$$R_{\mathrm{p}} = \frac{p_{\mathrm{sat}}(T_{\mathrm{inj}})}{p_{\mathrm{c}}} \tag{3}$$

with the saturation pressure p_{sat} at T_{inj}. The cryogenic temperature adjustment and injection system consists of a double-walled, vacuum-insulated pressure tank filled with liquid and gaseous nitrogen. Inside this nitrogen tank is the complete cryogenic feed and injection system, which is a 0,5 l LN2/LOX run tank, a mass flowmeter, a pneumatic run valve, the injector nozzle and piping in between, see Figure 2 in the middle. All these sub-systems are surrounded by the cooling medium nitrogen to provide a homogenous temperature distribution from the run tank to the injector nozzle.

The temperature regulation is realized by pressurizing the pressure tank surrounding the actual injection system with LN2/GN2 (gaseous nitrogen): By evacuation or pressurization of the gaseous nitrogen phase in the pressure tank, the fluid is cooled down or heated up, respectively. In the first case, a new saturation state is reached due to vaporization of a certain amount of LN2. The latent heat of vaporization necessary for this phase change leads to a loss of heat of the LN2/GN2 and consequently to a temperature decrease. In the second case, the saturation state after pressurization with gaseous nitrogen is reached due to condensation of the latter. In this process the latent heat of vaporization is released and heats the nitrogen. Several pressure and temperature sensors are installed in the nitrogen pressure tank as well as in the LN2/LOX feed and injection system, in order both to control and adjust the temperature of the cooling medium and to measure the injection parameters of the investigated jets. The knowledge of the injection parameters is particularly important for further numerical studies. A hand hole at the top of the nitrogen pressure tank provides the feedthroughs for the sensors and the supply pipes for the test medium nitrogen or oxygen as well as helium. The latter is used for the pneumatic actuation of the run valve, for purging and for the pressurization of the sensor cable ducts. The test medium enters the run tank in its gaseous state and is liquefied there by the surrounding cooling fluid of the LN2 pressure tank. Furthermore, the injection system allows a variation of the injector diameter by an exchange of the nozzle. The main parameters of the cryogenic temperature adjustment and injection system of the test bench M3.3 are: injection temperature $T_{inj} = 77 - 120\ \mathrm{K}$, injection

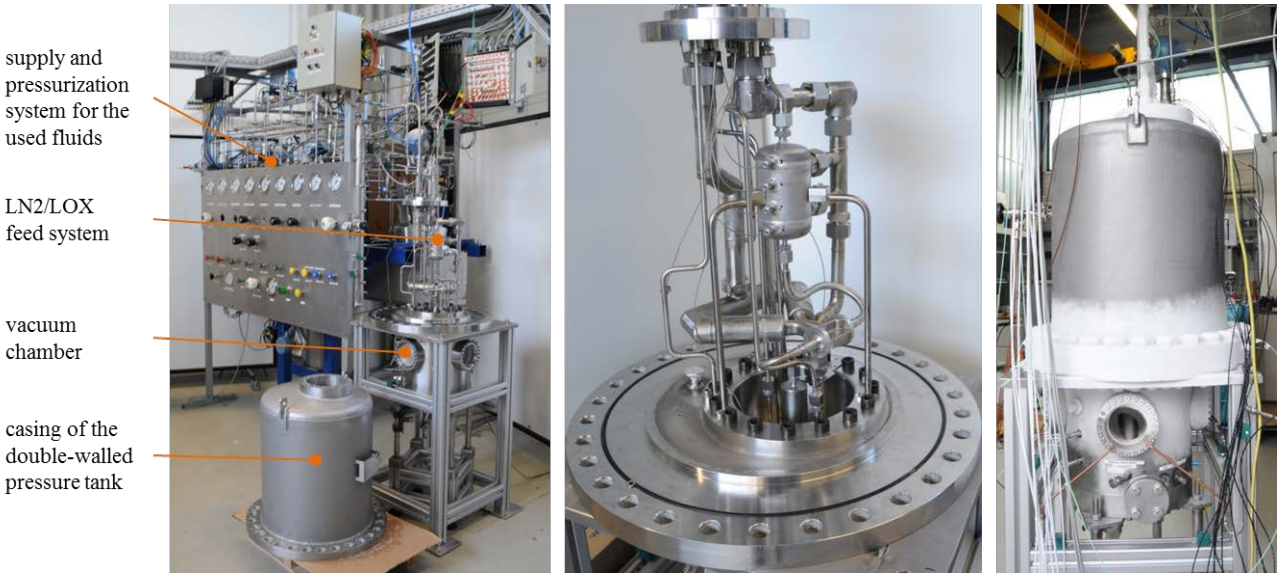

Figure 2: DLR test bench M3.3 with cryogenic injection system; left: test bench with main systems; middle: internal parts of the cryogenic temperature adjustment and injection system; right: chilled-down test bench.

pressure $p_{inj} = 1 - 20\ \mathrm{bar}$, back pressure $p_c = 0.005 - 1\ \mathrm{bar}$, injector diameter $D_{inj} = 0.2 - 1.3\ \mathrm{mm}$ and mass flow $\dot{m} = 0.08 - 50\ \mathrm{g/s}$.

The cryogenic temperature adjustment and injection system is mounted on top of the third main system, which consists of a vacuum chamber with four cylindrical windows for optical access and a vacuum pump. The LN2/LOX jets are injected vertically into the chamber and the resulting spray patterns are visualized via high-speed shadowgraphy (Photron FASTCAM SA-X with 10 000 fps and a resolution of 1024x1024 pixels) and with a phase Doppler (PD) system (Dantec High Dense Dual Mode system) to determine the size and velocity distributions of the droplets in the sprays. In a first measurement campaign, liquid nitrogen was used as test fluid with the high-speed shadowgraphy optical set-up to obtain the morphology of the resulting sprays. For all single test cases of that campaign the same injector with a diameter of D_{inj} = 1 mm was used. By variation of the back pressure and a constant injection temperature T_{inj} or by the variation of T_{inj} while p_c = const the three different breakup regimes *aerodynamical breakup*, *transition* and *fully flashing* according to Cleary *et al.* [26] were achieved. The shadowgraphs of one of these parameter sets is depicted in Figure 4. For these series of test cases the back

pressure was reduced gradually which leads to an increase of the degree of superheat R_p, see Equation (3). The LN2 jets were injected into the vacuum chamber at a back pressure p_c in the range of 0.04 bar < p_c < 0.6 bar at the constant injection conditions T_{inj} = 82.5 K (±0.6 K) and p_{inj} = 8 bar (±0.4 K). From the top left to the bottom right in the figure the resulting sprays become wider and ligaments of the liquid phase shrink until they disappear completely at high degrees of superheat $R_p \geq \approx 12$, where the so-called fully flashing regime is reached.
At smaller superheats 3 < R_p < 12 the sprays are in the transition regime between the aerodynamical breakup and the fully flashing where the characteristics of both breakup patterns are visible. In a second measurement campaign LN2 sprays only in the fully flashing regime were investigated with the PD system to determine diameter and velocity distributions of the sprays. In Figure 5 on the left the distribution of the Sauter mean diameter D_{32} is shown at an axial distance of y/D = 40.4 from the injector outlet and at the radial position x/D = 0 for varying injection temperatures T_{inj}. As can be seen an increase of the injection temperature leads to smaller droplets. This is due to an increase of the degree of superheat which results in a more violent jet breakup by flash-evaporation. On the right side of the figure the D_{32} distribution is shown for constant injection conditions at different spray positions. In the spray center there is a local minimum followed by a local maximum in the near lateral regions before the droplets decrease farer away. With increasing distance to the injector outlet the droplet diameters increase and their distribution becomes more inhomogeneous.

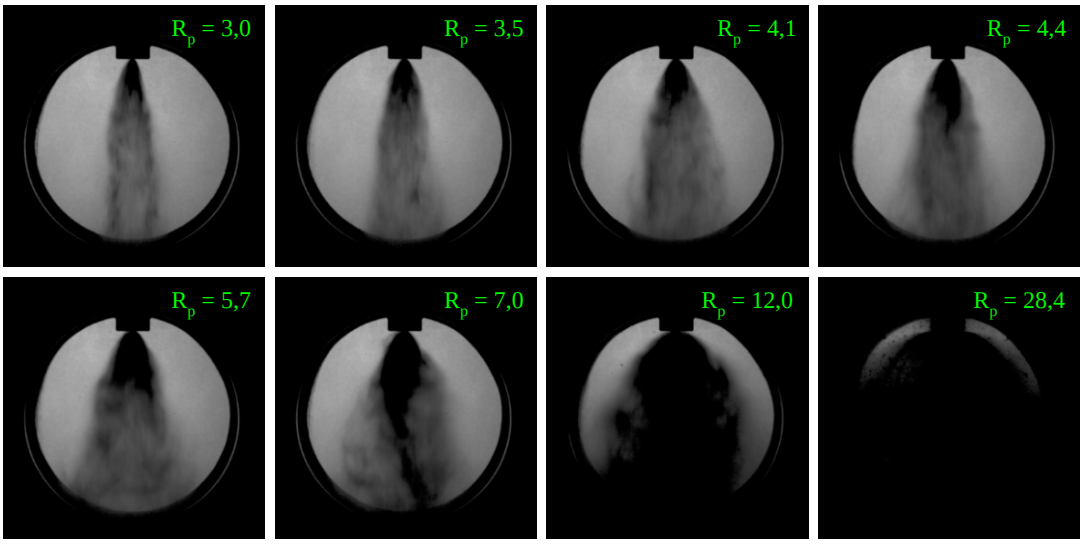

Figure 4: Shadowgraphy images of LN2 sprays at T_{inj} = 82.5K and p_{inj} = 8 bar for varying back pressures p_c (200 ms after opening the run valve).

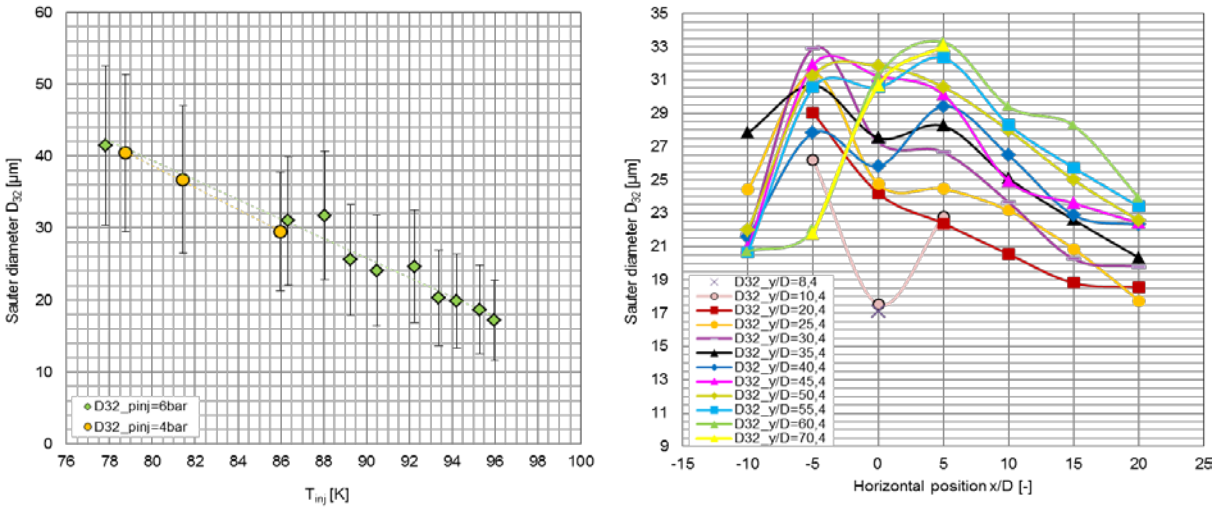

Figure 5: Sauter mean diameter D_{32} distribution for fully flashing LN2 sprays; left: D_{32} distribution at a constant spray position with varying injection temperature; right: D_{32} distribution at different spray positions for constant injection conditions

Drop impact and evaporation onto a heated wall in saturated vapor atmosphere
(TP-C1, TP-C2 T. Gambaryan-Roisman, A. Gholijani, C. Schlawitschek, P. Stephan, Institute for Technical Thermodynamics, TU Darmstadt)

If a drop hits a superheated wall, strong temperature gradients occur especially at the 3-phase contact line region where solid, liquid and vapour meet. Both, the hydrodynamics and the heat transfer are influenced by processes in the vicinity of the 3-phase contact line. Additionally, applying high pressure changes the physical properties of the fluid and therefore influences the physical behaviour of the drop impact and evaporation process. The objective of TP-C1 is to investigate the influence of high pressure during drop impact on hot walls. In TP-C1, the description of local nano- and micro-scale phenomena in the vicinity of the 3-phase contact line is coupled with a VOF code for modeling the macroscopic heat and fluid flow using OpenFOAM. Current activities aim for the implementation of a compressible fluid flow instead of the assumption of the incompressibility for both phases, liquid and vapour. The influence of the Kapitza resistance (thermal resistance at the solid-liquid interface) on the evaporation in the vicinity of a 3-phase contact line in a continuum theory context was investigated in cooperation with the TP-A4 [27]. Numerical studies of the heat transfer during simultaneous impact of two drops onto a hot solid substrate were performed in cooperation with the TP-C4 [29]. Lately, a feasibility study of the incompressible solver for simulation of drop impact and evaporation at high-reduced pressures was conducted [29]. Figure 6 shows snapshots shortly before drop impact (left) and during the drop spreading phase (right). Current activities focus on the influence of high pressure on both, micro- and macro-length scales.

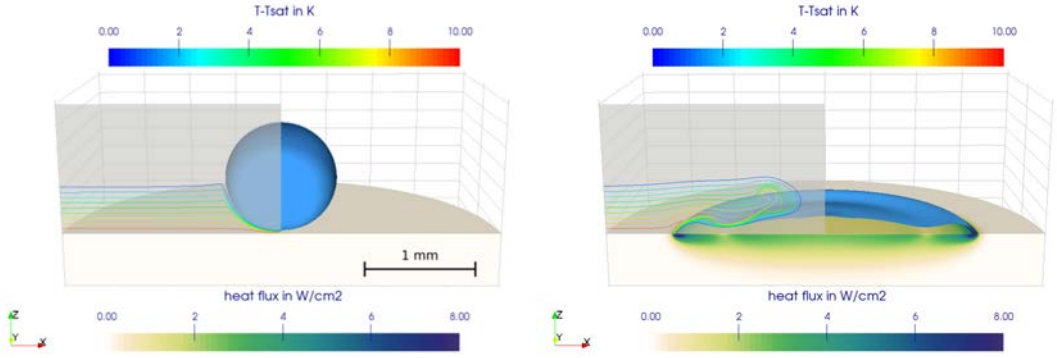

Figure 6: Drop impact at *a* $p=6p_{atm,}$ $(T_{wall} - T_{sat})$ = 10K, D_0 =1mm, u_0 = 0.25m s^{-1}.

On the microscopic length scale (micro region), a strong influence of the latent heat of vaporization, the thermal conductivity and heat capacity of the liquid on the heat transfer are present. Heat transport in the micro region is governed by three thermal resistances, namely the resistance due to evaporation at the liquid/vapour interface, the heat conduction resistance within the liquid, and the solid-liquid interface resistance (Kapitza resistance). The liquid/vapour interface heat resistance shows a local minimum in an interval of p/p_{cr}=0.3...0.7. The heat resistance of the liquid film increases with increasing pressures. The Kapitza resistance is independent of the pressure in the range of interest. The influence of pressure on transport processes in the micro region has been studied by numerical simulations. The wall superheat and contact line velocities are chosen in such a way that the assumptions of the mathematical model are fulfilled in a wide pressure range, and the contact line velocities occurring in the macro CFD model are met. Both, for the static and moving contact lines, the apparent contact angle increases with increasing pressures. Due to an increasing overall thermal resistance, the integrated heat flux per contact line length decreases. If pressure increases, the physical properties change. To account for the compressibility of the vapour and the liquid, a compressible solver of the OpenFOAM package is utilized and step-wise modified. A verification of the evaporation model by comparison with the results from literature has been performed. Scriven [30] reported an analytical solution for the bubble growth dynamics in superheated liquid due to evaporation. The assumptions of the analytical model include: incompressible fluid, negligible gravitational and surface tension forces. In order to compare the solver enhanced by the evaporation model with the results of [30], it has been run with constant density fluid model.

The subproject C2 is devoted to high-resolution experimental investigation of the hydrodynamics and heat transfer during drop impact onto a hot wall in a saturated vapour atmosphere. The wall superheat and impact velocity are varied during the experiment. The outcome of drop impact and the associated transport phenomena are determined by the Jacobs, Reynolds, Weber, Prandtl and Bond numbers.

The setup benefited from a temperature controlled test cell, which allows the drop impact investigations under a pure vapour atmosphere, and a syringe pump to generate reproducible drops by pumping the working fluid from a reservoir to a needle. Refrigerant FC-72 (perfluorohexane) is used as the working fluid. The experiments have been performed at a cell temperature of $T_{sat} = 328.15\ \mathrm{K}$, which corresponds to the saturation pressure of 0.95 bar. The substrate consist of a 400 nm chromium (Cr) layer as a Joule heating layer on top of a 400 nm high emissive chromium nitride (CrN) layer, which both are sputtered onto an infrared-transparent glass (CaF_2). The variation of

wall superheat ($T_w - T_{sat}$) is realized by varying the electrical power supplied to the Cr layer. The impact velocity, u_0, is varied by installing the needle at different heights. The temperature field of the heated surface can be directly observed by an infrared camera through the infrared-transparent glass from below. A finite volume method is used to compute the time-dependent heat flux distribution at the solid-fluid interface from the temperature field by solving transient three-dimensional heat conduction equation. The total heat flow, $\dot{Q}$, is evaluated by integration of the local heat flux across the drop footprints. The temporal evolution of contact diameter, D_{cl}, is derived with the image post-processing. The drop diameter and the impact velocity are derived by post-processing of the side view images, captured with a high-speed B/W camera. The results below are reported in dimensionless form. The relevant dimensionless variables and parameters are dimensionless time, spreading ratio, dimensionless heat flow, Reynolds, Weber, Jacobs, Bond and Prandtl numbers, which are defined by:

$$\tau = \frac{u_0 t}{D_0},\ \mathrm{S} = \frac{D_{cl}}{D_0},\ \dot{Q}^* = \frac{6\dot{Q}}{\pi \rho_l D_0^2 u_0 h_{lv}},\ \mathrm{Re} = \frac{\rho_l u_0 D_0}{\mu_l},\ \mathrm{We} = \frac{\rho_l u_0^2 D_0}{\sigma},\ \mathrm{Ja} = \frac{c_l (T_w - T_{sat})}{h_{lv}},\ \mathrm{Bo} = \frac{\rho_l g D_0^2}{4\sigma},\ \mathrm{Pr} = \frac{c \mu_l}{k}.$$

In these equations t denotes the time, ρ_l, μ_l, c_l and k_l are the liquid density, dynamic viscosity, specific heat capacity and thermal conductivity, σ denotes the surface tension, h_{lv} denotes the latent heat of evaporation, D_0 denotes the impact diameter, and g is the gravity acceleration. The drop impingement event can be subdivided into three phases: (i) the droplet spreading phase, where inertia forces dominate, (ii) the receding phase, where surface tension dominates, and (iii) the sessile droplet phase. During all phases heat is transferred by conduction, convection and partial evaporation, however the contribution of each mechanism differs. Figure 7 depicts the spreading ratio and heat transfer evolution for various wall superheats (ranged from 5.5 to 16.5 K) and subsequently Ja numbers. Larger Ja numbers lead to a reduction of the maximum spreading ratio and to a significantly shorter drop receding phase. A strong oscillation of the spreading ratio at the end of the receding phase is observed as well. An increase of Ja numbers lead to larger dimensionless heat flows. However, this increment is weaker than linear due to the decrease of wetted area by increasing wall superheat. Figure 8 illustrates the spreading ratio and the heat transfer evolution for various impact velocities (ranging from 0.33 to 0.57 ms^{-1}) and accordingly Re and We numbers. If both Re and We numbers increase, the maximum of the spreading ratio increases as well and is reached at a larger dimensionless time. Additionally, lower dimensionless heat flow is measured during the whole spreading phase and a part of the receding phase if both Re and We increase. This trend agrees with the theoretical predictions of [31].

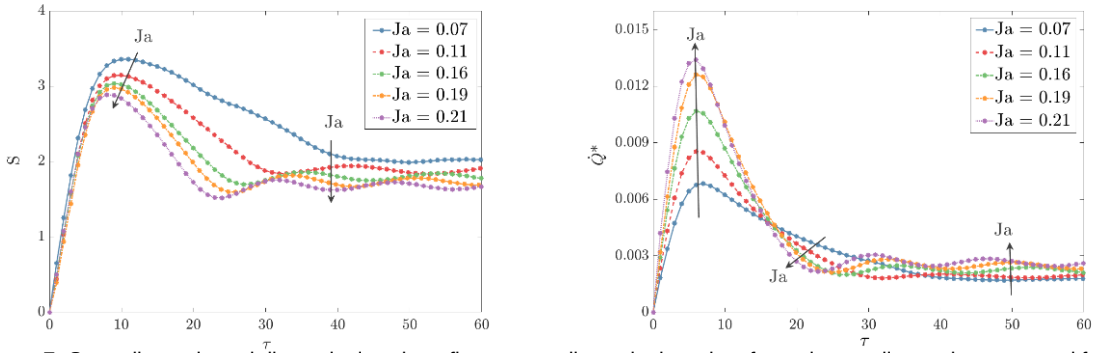

Figure 7: Spreading ratio and dimensionless heat flow versus dimensionless time for various wall superheats ranged from 5.5 to 16.5 K, (Re= 1513, We= 41, Bo= 1.7 and Pr= 9.7).

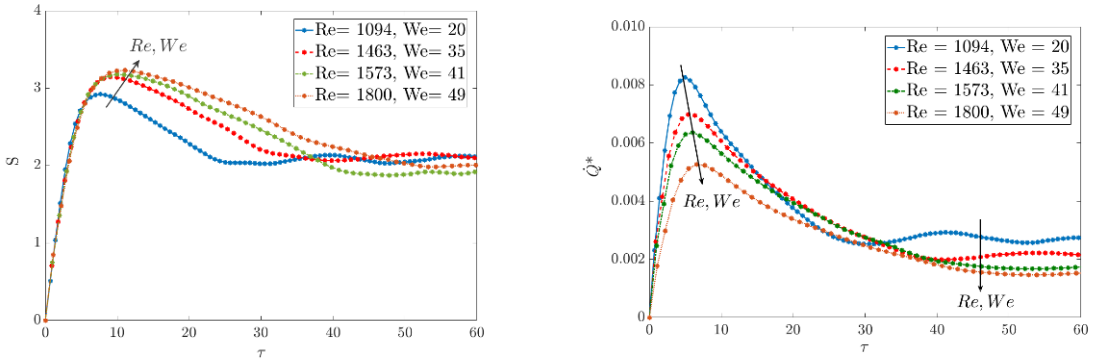

Figure 8: Spreading ratio and dimensionless heat flow versus dimensionless time for various impact velocities ranged from 0.33 to 0.57 m.s^{-1}, (Ja= 0.07, Bo= 1.7 and Pr= 9.7).

Conclusions

This paper has shown the structure of and the work carried out in the Collaborative Research Center SFB-TRR 75: “Droplet Dynamics under Extreme Ambient Conditions”. The work in the current funding period of this CRC focuses on large number of drops and in many instances on the behaviour and application of sprays under extreme ambient conditions. In this funding period further projects involving industrial participation are planned.

Acknowledgements

The members of the SFB-TRR 75 would like to thank the Deutsche Forschungsgemeinschaft (DFG) for the financial support of the SFB-TRR 75.

References

[1] Plateau, J.A.F., Statique. *Gauthier & Villars*, Paris (1873).
[2] Rayleigh, Lord J.S.W., *Proc. London Math. Soc.* 10, pp. 4-13 (1878).
[3] Pruppacher, H.R., Klett, J.D., Microphysics of Clouds and Precipitation. Reidel Publ., Dordrecht (1978).
[4] Lefebvre, A.H., Atomization and Sprays. Combustion: An International Series. Hemisphere Publishing Corporation, New York (1989).
[5] A. Frohn, N. Roth., Dynamics of Drops. Springer-Verlag, Heidelberg (2000).
[6] Tropea, C., Weigand, B., ICLASS 2015, Tainan, Taiwan (2015)
[7] Weigand, B., Tropea, C., Schulte, K., ILASS-Europe, Brighton, UK (2016)
[8] Tropea, C., Weigand, B. Schulte, K. ILASS-Europe, Valencia, Spain (2017)
[9] Schulte, K., Weigand, B., Tropea, C. ICLASS, Chicago, US (2018)
[10] Hindenlang, F., Gassner, G., Altmann, C., Beck, A., Staudenmaier, M., Munz, C.-D., Computes & Fluids, 61, pp. 86-93 (2012).
[11] Toro, E., “Riemann Solvers and Numerical Methods for Fluid Dynamics”, (2009).
[12] Kennedy, C., Carpenter, M., Lewis, R., Applied Numerical Mathematics, 35.3, pp. 177-219, (2008).
[13] Sonntag, M., Munz, C.-D., Journal of Scientific Computing, 70.3, pp. 1262-1289, (2017).
[14] Sussman, M., Smereka, P., Osher, S., Journal of Computational Physics, 114.1, pp. 146-159, (1994).
[15] Dumbser, M., Computers & Fluids, 39.1, pp. 60-76, (2010).
[16] Jiang, G.-S., Peng, D., SIAM Journal on Scientific Computing, 21.6, pp. 2126-2143,(2010).
[17] Adalsteinsson, D. Sethian, J. A., Journal of Computational Physics, 148, pp. 2-22, (1999).
[18] Föll, F., Hitz, T., Müller, C. Munz, C.-D., Dumbser, M., Shock Waves, accepted, (2019).
[19] Dumbser, M., Iben, U., Munz, C.-D., Computers & Fluids, 86, pp. 141-168, (2013).
[20] Bell, I. Wronski, J., Quoilin, S., Lemort, V., Industrial & Engineering Chemistry Research, 53.6, pp. 2498-2508, (2014).
[21] Fechter, S., Jaegle, F., Schleper, V., Computers & Fluids, 75, pp. 112-126, (2013).
[22] Fechter, S., Munz, C.-D., Rohde, C., Zeiler, C., Journal of Computational Physics, 336, pp. 347-374, (2017).
[23] Fechter, S., Munz, C.-D., Rohde, C., Zeiler, C., Computers & Fluids, 169, pp. 169-185, (2018).
[24] Jägle, F., Rohde, C., Zeiler, C., ESAIM Proceedings, 38, pp. 387-408, (2013).
[25] Hu, X., Adams, N., Iaccaino, G., Journal of Computational Physics, 228.17, pp. 6572-6589, (2009).
[26] Cleary, V., Bowen, P., Witlox, H.: Flashing liquid jets and two-phase droplet dispersion - I. Experiments for derivation of droplet atomization correlations. *J. Hazard. Mater.*, 142:786-796, (2007).
[27] Han, H.,Schlawitschek, C., Katyal, N., Stephan, P., Gambaryan-Roisman, T., Leroy, F., Müller-Plathe, F., *Langmuir* , 33 (21),pp. 5336-5343 (2017)
[28] Batzdorf, S., Breitenbach, J., Schlawitschek, C., Roisman, I., Tropea, C., Stephan, P., Gambaryan-Roisman, T., *Int. J. Heat Mass Transfer* (113): pp. 898-907 (2017)
[29] Schlawitschek, C., Stephan, P., Gambaryan-Roisman, T.: GVC-Tagung Wärme- und Stoffübertragung, Bremen, Germany (2018)
[30] Scriven, L.E., *Chem. Engng Sci*. (10), pp. 1-13 (1959)
[31] Herbert, S., Gambaryan-Roisman, T., Stephan, P., Colloids and Surfaces A (432), pp. 57-63 (2013)